Research Article | Vol. 12, No. 11 / 1 Nov 2021 / Biomedical Optics Express 7173
Biomedical Optics EXPRESS

Quantitative multi-height phase retrieval via a coded image sensor

CHENGFEI GUO,[1,2] SHAOWEI JIANG,[2] PENGMING SONG,[2] TIANBO WANG,[2] XIAOPENG SHAO,[1,4] ZIBANG ZHANG,[3] AND GUOAN ZHENG[2,5]

[1]Xi'an Key Laboratory of Computational Imaging, Xidian University, Shaanxi 710071, China
[2]Department of Biomedical Engineering, University of Connecticut, Storrs, CT 06269, USA
[3]Department of Optoelectronic Engineering, Jinan University, Guangzhou 510632, China
[4]xpshao@xidian.edu.cn
[5]guoan.zheng@uconn.edu

Abstract: Multi-height phase retrieval introduces different object-to-detector distances for obtaining phase diversity measurements. In the acquisition process, the slow-varying phase information, however, cannot be converted to intensity variations for detection. Therefore, the low-frequency contents of the phase profile are lost during acquisition and cannot be properly restored via phase retrieval. Here, we demonstrate the use of a coded image sensor for addressing this challenge in multi-height phase retrieval. In our scheme, we add a coded layer on top of the image sensor for encoding the slow-varying complex wavefronts into intensity variations of the modulated patterns. Inspired by the concept of blind ptychography, we report a reconstruction scheme to jointly recover the complex object and the unknown coded layer using multi-height measurements. With both simulation and experimental results, we show that the recovered phase is quantitative and the slow-varying phase profiles can be properly restored using lensless multi-height measurements. We also show that the image quality using the coded sensor is better than that of a regular image sensor. For demonstrations, we validate the reported scheme with various biospecimens and compare the results to those of regular lensless multi-height phase retrieval. The use of a coded image sensor may enable true quantitative phase imaging for the lensless multi-height, multi-wavelength, and transport-of-intensity equation approaches.

1. Introduction

Light detectors such as image sensors and photographic plates can only measure intensity variations of the light that hits them. In the process of recording, they lose the phase information, which characterizes how much the light is delayed through propagation. Phase retrieval is a technique to recover the lost phase information based on one or more distinct intensity measurements. It typically consists of iteratively reinforcing these known intensities while an initially random phase "guess" is allowed to converge to a solution that matches all measurements [1]. Robust phase retrieval is typically performed by introducing different types of diversity measurements [2], including defocus multi-height diversity [3–7], multi-wavelength diversity [8–10], transverse translational diversity in the spatial [11–14] and the Fourier domain [15,16], nonlinear diversity [17], among others.

In defocus multi-height phase retrieval, different object-to-detector distances are adopted for obtaining phase diversity measurements. This concept, also termed 'focus series reconstructions' was first introduced in 1968 for electron microscopy [3]. In the optical region, it has been demonstrated in wavefront reconstruction [4,5] and shows great potentials for lensless on-chip microscopy [6,7]. In a typical implementation, the specimen is axially translated to different defocus distances and the diffraction patterns are recorded using a regular image sensor. In the

#443528 https://doi.org/10.1364/BOE.443528
Journal © 2021 Received 16 Sep 2021; revised 12 Oct 2021; accepted 13 Oct 2021; published 29 Oct 2021

Biomedical Optics EXPRESS

reconstruction process, the complex object estimate is iteratively propagated to these different defocus planes and the captured images are enforced as magnitude constraints. In this approach, however, the slow-varying phase information cannot be converted into intensity variations for detection. This effect can be explained by the phase transfer function (PTF), which characterizes the transfer property of phase contents at different spatial frequencies [18]. For low-frequency contents, PTF is close to 0 under the weak phase approximation. As a result, these contents are lost during acquisition and cannot be restored in the post-acquisition phase retrieval process.

Here we demonstrate the use of a coded image sensor for addressing this challenge in multi-height phase retrieval. In our scheme, we add a coded layer on top of the image sensor for encoding the slow-varying waves into intensity variations of the modulated patterns. Inspired by the concept of blind ptychography [12,13,19–23], we report a reconstruction scheme to jointly recover the complex object and the unknown coded layer using multi-height measurements. With both simulation and experimental results, we show that the recovered phase is quantitative and the slow-varying phase profiles can be properly restored in post-acquisition reconstruction. We also show that the image quality using the coded sensor is better than that using a regular image sensor. For demonstrations, we validate the reported scheme with biospecimens and compare the results to those of regular lensless multi-height retrieval. The use of coded image sensor may enable true quantitative phase imaging for the lensless multi-height, multi-wavelength, and transport-of-intensity equation approaches.

This paper is structured as follows: In Section 2, we will first discuss the imaging model of the multi-height coded imaging setup and propose a joint reconstruction scheme for recovering both the complex object and the unknown coded layer. In Section 3, we will demonstrate the simulation results and show that it is challenging to recover the slow-varying phase information using the regular defocus multi-height approach. We will also show that the multi-height coded imaging setup can address this critical challenge and enables quantitative phase recovery. In Section 4, we will validate the effectiveness of the reported scheme using known quantitative targets and compare the results to the regular multi-height approach. In Section 5, we will test our reported scheme with biospecimens. Finally, we will summarize the results and discuss the future directions in Section 6.

2. Imaging model and the proposed joint recovery scheme

Figure 1 shows the comparison between the conventional multi-height phase retrieval and the proposed coded sensor scheme. For both approaches, the object is translated along the axial direction for diffraction data acquisition. In the conventional multi-height approach, a regular image sensor is used to record the intensity variations on the detector plane (Fig. 1(a2)). In this approach, the slow-varying phase information cannot be converted into intensity variations for detection. In the proposed scheme, we used a coded image sensor shown in Fig. 1(b2) for image acquisition.

The concept of coded image sensor shares its root with coded diffraction imaging where a known programmable phase mask is placed behind the object for light modulation [24,25]. In practice, it is challenging to have precise knowledge of the complex profile, the alignment, and the programmable change of the mask behind the object [26]. It also shares some similarity with the use of pseudo random masks and physical layers to improve coherent imaging and phase retrieval [27–29]. In our implementation, we directly add a coded layer on top of a regular image sensor, similar to the configuration of FlatScope [30] or DiffuserCam [31] but with an unknown complex mask and operated in a coherent imaging setting. The forward imaging model of the proposed system shown in Fig. 1(b1) can be described as:

$$I_j(x,y) = \left|\left(O(x,y) * PSF_{free}(d_j)\right) \cdot S(x,y) * PSF_{free}(d_0)\right|^2_{\downarrow M}, \tag{1}$$

Biomedical Optics EXPRESS

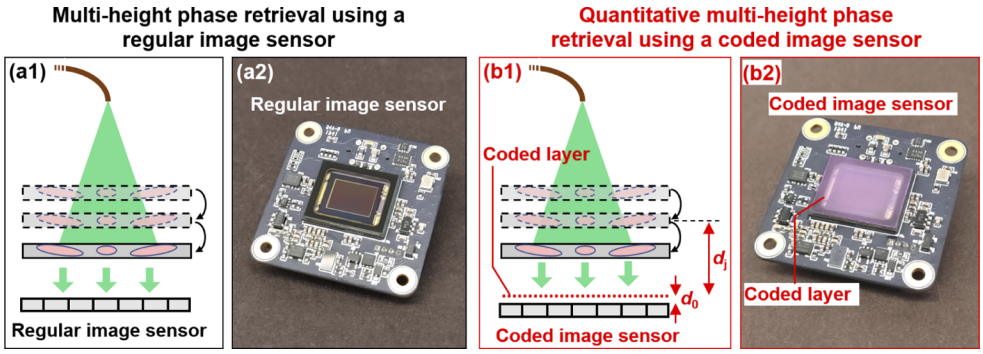

Fig. 1. The comparison between the conventional multi-height phase retrieval (a) and the proposed scheme using a coded image sensor (b). The requirement for the coded layer is a thin but dense layer that provides adequate modulation of the impinging light waves and can be modelled by a multiplication process in Eq. (1).

Algorithm outline

Input: Raw images I_j $(j = 1,2,\cdots,J)$ captured at different defocus distances d_j
Output: High-resolution object $O(x,y)$ and the coded layer profile $S(x,y)$

1. Initialize $O(x,y)$ and $S(x,y)$
2. **for** n= 1: N (different iterations)
3. **for** j = 1: J (different captured images)
4. $W_j(x,y) = PSF_{free}(d_j) * O(x,y)$ % Propagate the object to the coded layer plane
5. $\phi_j(x,y) = S(x,y) \cdot W_j(x,y)$ % Exit wave on the coded layer plane
6. $\psi_j(x,y) = PSF_{free}(d_0) * \phi_j(x,y)$ % Light on the image sensor plane
7. Update $\psi_j(x,y)$:
$$\psi_j'(x,y) = \psi_j(x,y) \cdot \frac{\sqrt{I_j(\lceil x/M \rceil, \lceil y/M \rceil)}}{\sqrt{U_j(\lceil x/M \rceil, \lceil y/M \rceil)}}$$ ('⌈ ⌉': the ceiling function; $U_j(x,y) = |\psi_j(x,y)|^2 * ones(M,M)$)
8. $\phi_j'(x,y) = PSF_{free}(-d_0) * \psi_j^{update}(x,y)$ % Propagate back to the coded layer plane
9. Jointly update the object exit wave $W_j(x,y)$ and the coded layer profile $S(x,y)$:
$$W_j^{update}(x,y) = W_j(x,y) + (conj(S(x,y)) \cdot \{\phi_j'(x,y) - \phi_j(x,y)\})/((1-\alpha_{obj})|S(x,y)|^2 + \alpha_{obj}|S(x,y)|^2_{max})$$
$$S^{update}(x,y) = S(x,y) + (conj(W_j(x,y)) \cdot \{\phi_j'(x,y) - \phi_j(x,y)\})/((1-\alpha_s)|W_j(x,y)|^2 + \alpha_s|W_j(x,y)|^2_{max})$$
10. Propagate the updated object exit wave back to the object plane: $O(x,y) = PSF_{free}(-d_j) * W_j^{update}(x,y)$
11. **end**
12. **end**

Fig. 2. The joint recovery scheme for coded multi-height phase retrieval. The complex object and the unknown coded layer can be jointly recovered from the multi-height measurements.

where $I_j(x,y)$ is the j^{th} intensity measurement by placing the object $O(x,y)$ at a distance d_j from the coded layer, PSF_{free} is the point spread function (PSF) for free-space propagation, $S(x,y)$ is the complex profile of the coded layer, d_0 is the distance between the coded layer and the sensor pixel array, and '$*$' denotes the convolution operation. We use '$\downarrow M$' to represent the down-sampling process of the image sensor. Based on all captured images $I_j(x,y)$, we aim to jointly recover the complex object $O(x,y)$ and the complex profile of the coded layer $S(x,y)$.

Figure 2 shows the workflow of the proposed joint recovery scheme for multi-height phase retrieval. We first initialize the amplitude of the object by averaging all captured measurements and set the phase to 0. We initialize the coded layer to an all-one matrix (i.e., assuming no diffusing layer for the initial guess). In the iterative reconstruction process, we first propagate the object to the coded layer with the corresponding distance and obtain wavefront $W_j(x,y)$ in line 4 of Fig. 2. We then multiply with the coded layer profile $S(x,y)$ to form an exit wave $\phi_j(x,y)$ in line

Biomedical Optics EXPRESS

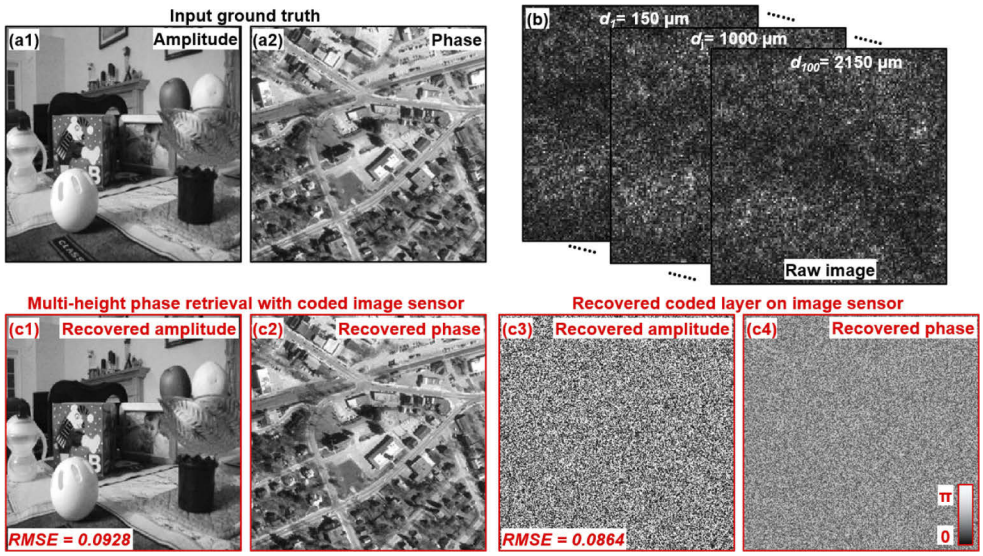

Fig. 3. Simulation of the joint recovery scheme for coded multi-height phase retrieval. (a) The input ground-truth object, with a maximum phase of π and a size of 256 by 256 pixels. (b) The simulated multi-height measurements captured by a coded image sensor. 100 raw images are used in this simulation, with a 20-μm step size along the axial direction. (c) The joint recovery of the complex object and the complex coded layer. A large number of raw images are only needed for the joint recovery process. Once the coded layer is determined from a calibration experiment, the number of raw images can be reduced to 10 or less for other specimens.

5. This exit wave is propagated to the image sensor plane to obtain the complex wave $\psi_j(x, y)$ in line 6. At the image sensor plane, we use the j^{th} intensity measurement $I_j(x, y)$ to update $\psi_j(x, y)$ in line 7. This updating process enforces the intensity summation of every M by M small pixel in the complex wavefront equals to the corresponding raw pixel in the captured image [13,32]. With the $\psi_j'(x, y)$, we then propagate it back to the coded layer plane and obtain the updated exit wave $\phi_j'(x, y)$ in line 8. In line 9, we modify the regularized ptychographical iterative engine (rPIE) [33] to update the object wavefront and the complex profile of the coded layer. The α_{obj} and α_s in the updating equation are algorithm weights in rPIE [33]. In line 10, we propagate the updated exit wave from the coded layer back to the object plane and obtain the updated object. This process is repeated for different measurements in line 11 and iterated in line 12.

Figure 3 shows the simulation study of the proposed joint recovery scheme. Figures 3(a) shows the input complex object, with the maximum phase of π. Figure 3(b) shows the simulated raw images captured using the coded image sensor with an unknown coded layer. The illumination wavelength is 532 nm and the pixel size is 1.85 μm (chosen based on our experimental setting). Based on the joint recovery scheme, Fig. 3(c) shows the recovered complex object and the coded layer, where we use 100 raw images for reconstruction. The defocus distance d_j ranges from 150 μm to 2150 μm, with a 20-μm step size. For all simulations, we also label the root mean square error (RMSE) between recovered complex images and the ground truths in the figures. We note that a large number of raw images are only needed for the joint recovery process. Once the coded layer is determined from a calibration experiment, the number of raw images can be reduced to 10 or less for other specimens (discussed in the next section).

Biomedical Optics EXPRESS

3. Multi-height phase retrieval performance on fast- and slow-varying phase profiles

In this section, we compare the imaging performance between the regular multi-height approach and the proposed multi-height coded phase retrieval. We focus on two different cases in simulation. The first one is a complex object with a fast-varying phase profile (Fig. 4). The second one is a complex object with a slow-varying phase profile (Fig. 5).

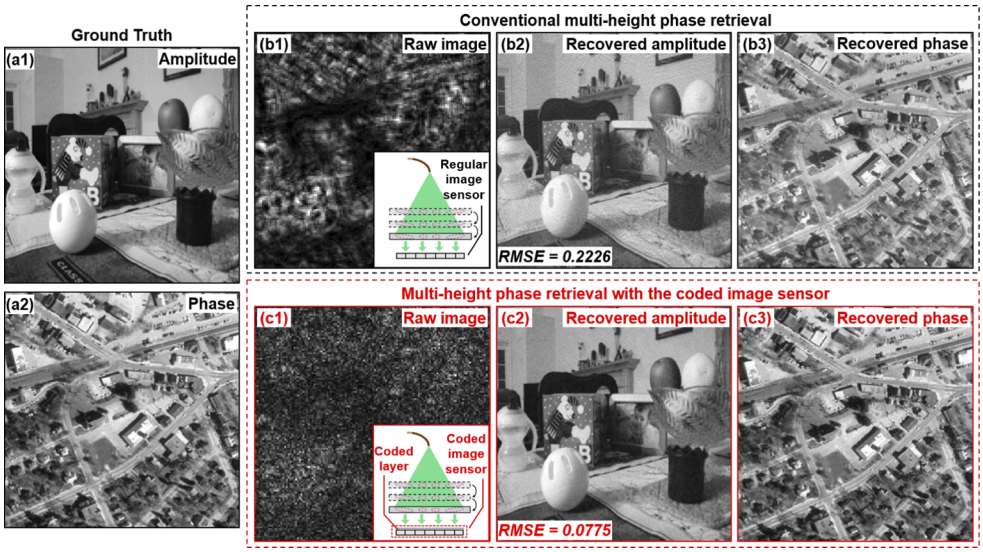

Fig. 4. Simulation of multi-height phase retrieval for fast-varying phase profile. (a) The input ground truth of amplitude and phase. The phase image contains fast-varying features. (b) The recovery using the conventional multi-height phase retrieval approach based on a regular image sensor (inset of (b1)). (c) The recovery using the proposed multi-height phase retrieval approach based on a coded image sensor (inset of (c1)). For both approaches, 10 raw images captured at different defocus distances are used to recover the complex object. The defocus distance d_j ranges from 150 μm to 330 μm, with a 20-μm step size.

For the first case, Fig. 4(a) shows the input complex image with the same parameters as those in Fig. 3. Figures 4(b) and 4(c) show the corresponding reconstructions using the two approaches. For both approaches, we use 10 raw images for reconstruction, and the defocus distance d_j ranges from 150 μm to 330 μm, with a 20-μm step size. We can see that both approaches can converge to the correct solution while the proposed coded sensor approach gives a better image quality.

For the second case, Fig. 5(a) shows the input complex image where the phase profile contains slow-varying content. If we unwrap the phase profile, the maximum phase value is 15 π in this simulation (inset of Fig. 5(a2)). Figures 5(b) and 5(c) show the corresponding reconstructions using the two approaches. We can see that the coded sensor approach can converge to the correct solution while the conventional multi-height approach fails. The inset of Fig. 5(c3) shows the unwrapped phase of the coded sensor recovery and the recovered phase in Fig. 5(b3) cannot be unwrapped.

In Fig. 6, we quantify the performance of the two approaches using the root mean square error (RMSE) metric. Figure 6(a) shows the convergence curves for the simulations in Fig. 4. We can see that the coded sensor approach performs better than that of the regular multi-height approach. Both curves in Fig. 6(a) decrease as the iteration increases, indicating good convergence performance. In contrast, Fig. 6(b) shows the convergence curves for the case of slow-varying phase profile in Fig. 5. In this case, the conventional multi-height approach fails to converge

Biomedical Optics EXPRESS

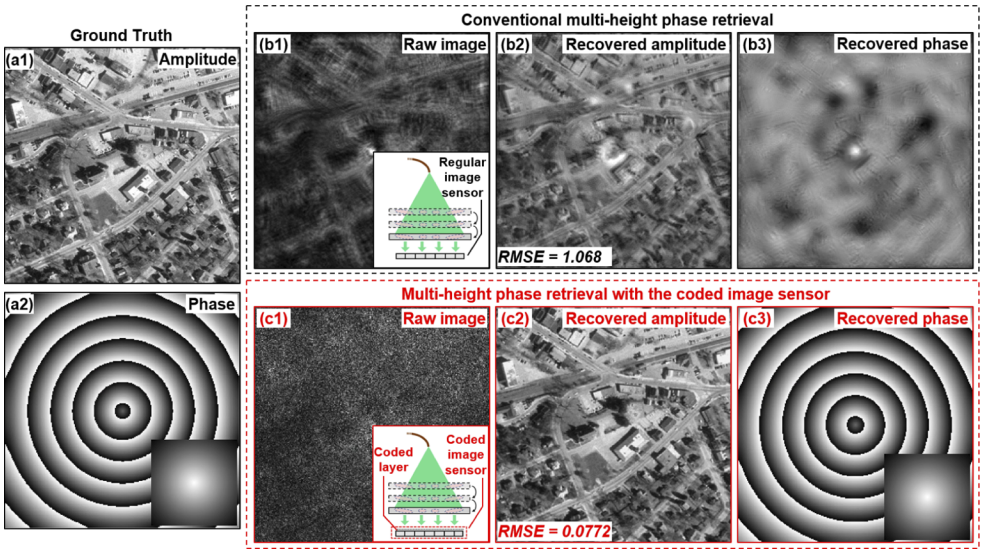

Fig. 5. Simulation of multi-height phase retrieval for slow-varying phase profile. (a) The input ground truth of amplitude and phase. The phase image contains slow-varying features. Inset of (a2) shows the unwrapped phase with the maximum phase value of 15 π. (b) The recovery using the conventional multi-height phase retrieval approach based on a regular image sensor (inset of (b1)). (c) The recovery using the proposed multi-height phase retrieval approach based on a coded image sensor (inset of (c1)). For both approaches, 10 raw images captured at different defocus distances are used to recover the complex object (same as Fig. 4). The coded image sensor approach can recover the slow-varying phase from the multi-height measurements while the conventional approach fails. Inset of (c3) shows the unwrapped phase while the phase of (b3) cannot be properly unwrapped.

while the proposed coded sensor approach can converge to the correct solution. The RMSE of the conventional multi-height is a constant in Fig. 6(b).

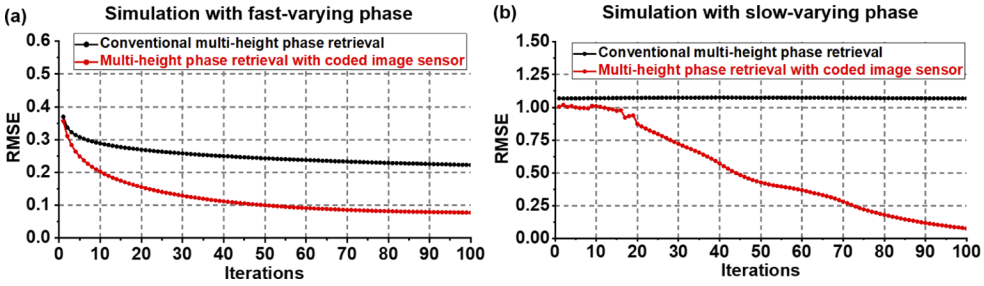

Fig. 6. Quantification of the multi-height phase retrieval simulations. (a) The two convergence curves for the fast-varying phase. Both approaches can converge to the correct solution while the proposed coded sensor approach has a better performance (red curve). (b) The two convergence curves for the slow-varying phase. The conventional multi-heigh approach fails to converge as the black curve does not decrease as the iteration increases. In contrast, the proposed coded sensor approach can converge to the correct solution.

The quantification in Fig. 6 can be explained using the PTF of defocus measurements [18]. Under the weak object approximation, low-frequency contents of the phase profile cannot be converted into intensity variation using a regular image sensor. As such, the slow-varying phase

Biomedical Optics EXPRESS

information is lost in the recording process, and it is challenging to restore it in post-acquisition processing. For the proposed coded image sensor, the low-frequency contents of the phase profile can be converted into the distortion of the modulated patterns via the coded layer. With a proper phase retrieval process, the slow-varying phase can be restored in the iterative reconstruction process.

4. Experimental validation using known quantitative targets

In this section, we validate the effectiveness of the proposed approach using quantitative targets. The coded layer is made by coating a thin layer of microbeads on top of the image sensor. In the calibration experiment, we use a blood smear sample as the object to jointly recover the object and the coded layer. Once the coded layer is recovered, we can compare the coded sensor approach with the regular multi-height approach to demonstrate its advantages.

In all following demonstrations, we use a monochromatic sensor with a 1.85-μm pixel size (Sony IMX 226) for image acquisition and a 532-nm laser diode for sample illumination. We capture 10 lensless raw images by translating the sample along the axial direction using a motorized stage. The step size is 20 μm, the same as that used in the simulation study. The acquisition time for 10 images is ~5 seconds without optimizing the speed. Figure 7 shows captured raw images and the reconstruction of a resolution target. Figure 7(a)–7(b) show the captured raw images and the reconstruction for the conventional multi-height approach. Figure 7(c)–7(d) show the captured raw images and the reconstruction for the coded sensor approach. Both approaches achieve a similar resolution performance while the coded sensor approach generates reconstruction with a more uniform background with fewer fringe artifacts.

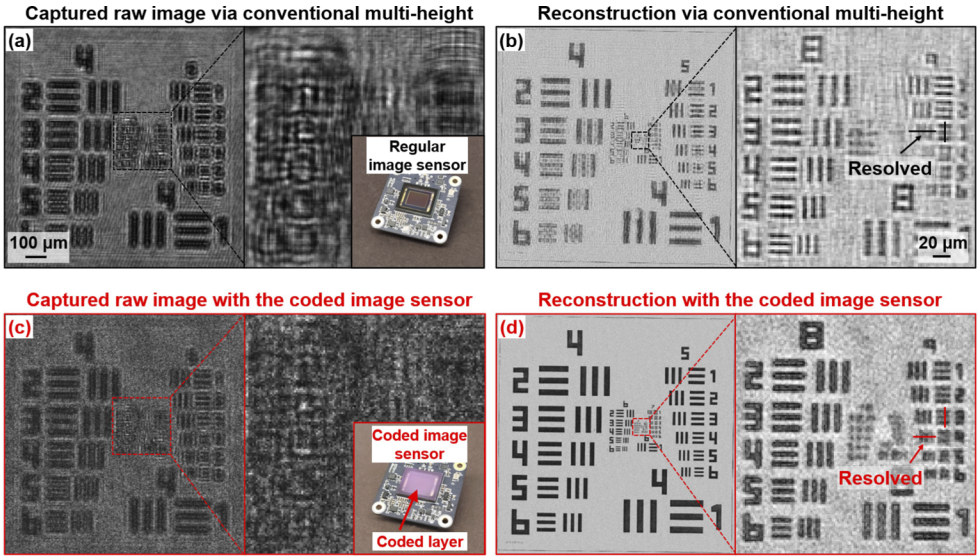

Fig. 7. Quantitative validation using a known resolution target. The raw image captured using the conventional multi-height approach (a) and the recovered intensity (b). The raw image captured using the coded sensor approach (c) and the recovered intensity (d).

A more interesting case for comparison is the performance of slow-varying phase profiles. Figure 8 shows captured raw images and the reconstruction for a quantitative phase target. Figure 8(a)–8(b) show the captured raw images and the reconstruction for the conventional multi-height approach. Figure 8(c)–8(d) show the captured raw images and the reconstruction for the coded sensor approach. The difference between these two approaches can be best visualized

Biomedical Optics EXPRESS

from the slow-varying phase features of the recovered images. In Fig. 8(e), we plot the line traces of a large square phase feature of the target. We can see that the conventional multi-height approach fails to recover the correct phase as shown in the green curves of Fig. 8(e). In contrast, the coded sensor approach can correctly recover such slow-varying features in a quantitative manner. This experiment validates the effectiveness of the proposed approach, and the conclusion is in good agreement with that of our simulation studies in Figs. 5–6.

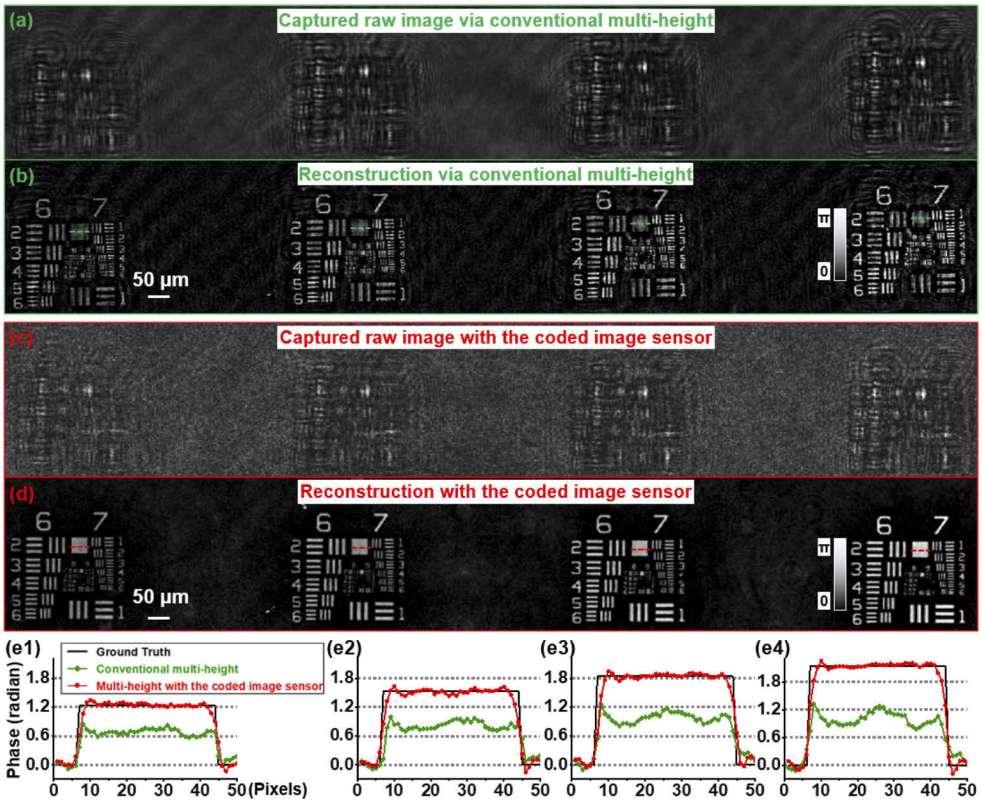

Fig. 8. Quantitative validation using a known phase target. The raw image captured using the conventional multi-height approach (a) and the reconstruction (b). The raw image captured using the coded sensor approach (c) and the reconstruction (d). (e) Line traces of the phase features.

5. Imaging performance on biospecimens with fast- and slow-varying phase profiles

In addition to the quantitative validation using known targets, we also qualitatively test both approaches with various biospecimens. Figure 9 shows the results on two biospecimens with fast-varying phase profiles: a histology slide with hematoxylin and eosin (H&E) stains and a blood smear. Figure 9(a1)-(a2) show the raw images captured using the conventional multi-height approach. Figure 9(a3)-(a4) show the raw images captured using the coded image sensor. The corresponding recovered amplitude and phase images are shown in Fig. 9(b)–9(c). We can see that both approaches can recover the object while the coded sensor approach has a better image quality.

In the second qualitative test in Fig. 10, we image a cultured bacterial colony with a slow-varying phase profile using both approaches. Figure 10(a1) shows the raw image captured

Biomedical Optics EXPRESS

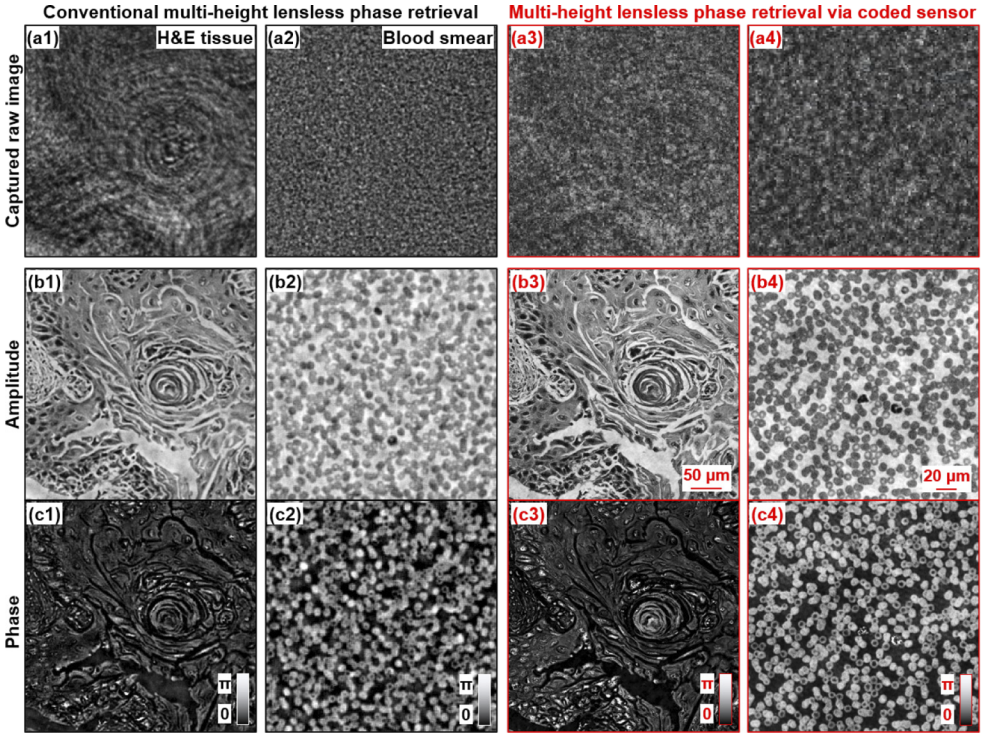

Fig. 9. Imaging performance demonstration using two biospecimens with fast-varying phase profiles. Captured raw images using the regular image sensor (a1-a2) and the coded image sensor (a3-a4). The corresponding reconstruction of the amplitude (b) and phase (c).

using the conventional multi-height approach. Figure 10(a2)-10(a3) show the corresponding recovered amplitude and phase images, and the reconstruction fails to converge to the correct solution. The recovered phase in Fig. 10(a3) cannot be properly unwrapped. In contrast with the conventional multi-height approach, Fig. 10(b1) shows the raw image captured using the coded sensor approach, and Fig. 10(b2)-10(b3) show the recovered amplitude and phase. In this case, we can recover the slow-varying phase of the bacterial colony and the background phase of the uneven agar plate can also be visualized from the fringe pattern in Fig. 10(b3). The inset of Fig. 10(b3) shows the unwrapped phase of the bacterial colony.

The imaging performance with biospecimens presented in this section agrees with the conclusion of the quantitative validation in the previous section. Both approaches can recover the fast-varying phase and the coded sensor approach has a better image quality. For a slow-varying phase profile, the conventional multi-height approach fails while the coded sensor approach can recover the low-frequency content of the object.

Biomedical Optics EXPRESS

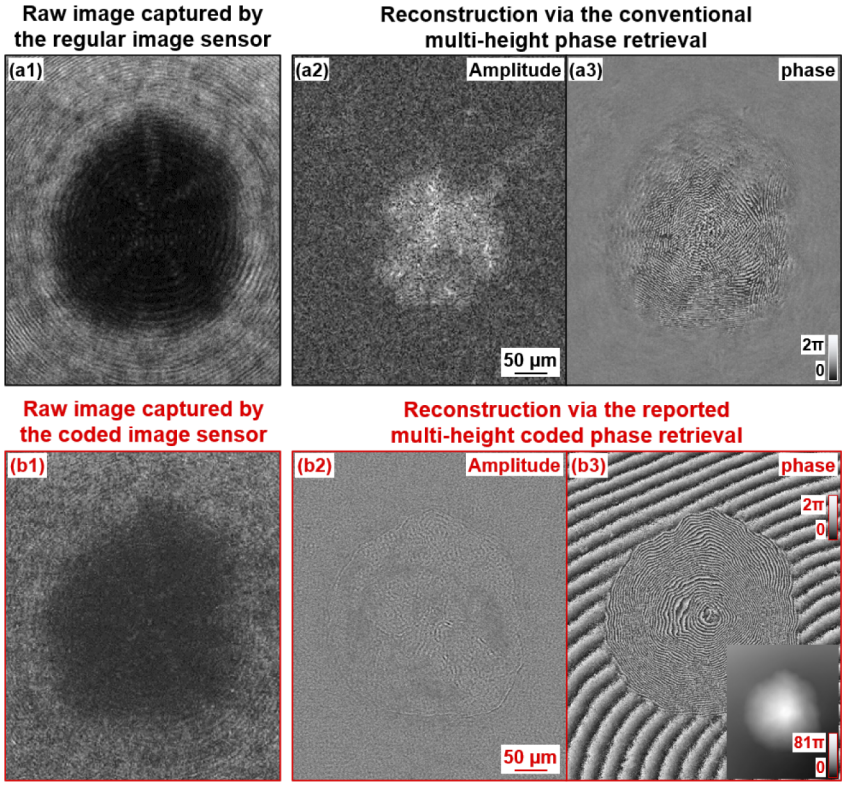

Fig. 10. Imaging performance demonstration using a cultured bacterial colony with slow-varying phase profile. (a1) The captured raw image using the regular image sensor. (a2-a3) The corresponding reconstruction of the amplitude and phase using the conventional multi-height approach. The recovered phase image cannot be unwrapped. (b1) The captured raw image using the coded image sensor. (b2-b3) The corresponding reconstruction of the amplitude and phase using the reported coded sensor approach. Inset of (b3) shows the unwrapped phase of the colony.

6. Summary and conclusion

In conventional multi-height phase retrieval, the slow-varying phase information cannot be converted into intensity variations for detection. This effect can be explained by the PTF, which is close to 0 for low-frequency contents. As a result, these contents are lost during acquisition and cannot be restored in the post-acquisition phase retrieval process. In this paper, we demonstrate the use of a coded image sensor for addressing this challenge in multi-height phase retrieval. In our scheme, we use a coded layer on the image sensor for encoding the slow-varying complex wavefronts into intensity variations of the modulated patterns. Inspired by the concept of blind ptychography, we report a reconstruction scheme to jointly recover the complex object and the unknown coded layer using multi-height measurements. With both simulation and experimental results, we show that the recovered phase is quantitative and the slow-varying phase profiles can be properly restored in post-acquisition reconstruction.

The approach presented in this work can also be used for other phase retrieval approaches. Our ongoing effort is to adopt the coded image sensor for multi-wavelength phase retrieval [8–10] and the transport-of-intensity approach [18]. The integration of coded image sensor in these approaches allows the low-frequency phase profile to be encoded in the intensity measurement, thereby enabling its recovery in the reconstruction process.

Biomedical Optics EXPRESS

Funding. 111 Project (B17035); National Natural Science Foundation of China (61975254).

Acknowledgment. Xiaopeng Shao acknowledges the 111 Project (B17035) and National Natural Science Foundation of China (NSFC) (61975254).

Disclosures. The authors declare no conflicts of interest.

Data availability. The data presented in this paper are not publicly available at this time but may be obtained from the authors upon reasonable request.

References

1. Y. Shechtman, Y. C. Eldar, O. Cohen, H. N. Chapman, J. Miao, and M. Segev, "Phase retrieval with application to optical imaging: a contemporary overview," IEEE Signal Process. Mag. **32**(3), 87–109 (2015).
2. J. R. Fienup, "Phase retrieval algorithms: a personal tour," Appl. Opt. **52**(1), 45–56 (2013).
3. P. Schiske, "Image reconstruction by means of focus series," in *Proceedings of the 4th European Conference on Electron Microscopy, Rome, Italy, 1968* (Tipografia poliglotta, 1968).
4. Y. Zhang, G. Pedrini, W. Osten, and H. J. Tiziani, "Whole optical wave field reconstruction from double or multi in-line holograms by phase retrieval algorithm," Opt. Express **11**(24), 3234–3241 (2003).
5. B. H. Dean and C. W. Bowers, "Diversity selection for phase-diverse phase retrieval," J. Opt. Soc. Am. A **20**(8), 1490–1504 (2003).
6. A. Greenbaum and A. Ozcan, "Maskless imaging of dense samples using pixel super-resolution based multi-height lensfree on-chip microscopy," Opt. Express **20**(3), 3129–3143 (2012).
7. A. Greenbaum, Y. Zhang, A. Feizi, P.-L. Chung, W. Luo, S. R. Kandukuri, and A. Ozcan, "Wide-field computational imaging of pathology slides using lens-free on-chip microscopy," Sci. Transl. Med. **6**(267), 267ra175 (2014).
8. P. Bao, F. Zhang, G. Pedrini, and W. Osten, "Phase retrieval using multiple illumination wavelengths," Opt. Lett. **33**(4), 309–311 (2008).
9. W. Luo, Y. Zhang, A. Feizi, Z. Göröcs, and A. Ozcan, "Pixel super-resolution using wavelength scanning," Light: Sci. Appl. **5**(4), e16060 (2016).
10. X. Wu, J. Sun, J. Zhang, L. Lu, R. Chen, Q. Chen, and C. Zuo, "Wavelength-scanning lensfree on-chip microscopy for wide-field pixel-super-resolved quantitative phase imaging," Opt. Lett. **46**(9), 2023–2026 (2021).
11. H. M. L. Faulkner and J. Rodenburg, "Movable aperture lensless transmission microscopy: a novel phase retrieval algorithm," Phys. Rev. Lett. **93**(2), 023903 (2004).
12. M. Guizar-Sicairos and J. R. Fienup, "Phase retrieval with transverse translation diversity: a nonlinear optimization approach," Opt. Express **16**(10), 7264–7278 (2008).
13. S. Jiang, J. Zhu, P. Song, C. Guo, Z. Bian, R. Wang, Y. Huang, S. Wang, H. Zhang, and G. Zheng, "Wide-field, high-resolution lensless on-chip microscopy via near-field blind ptychographic modulation," Lab Chip **20**(6), 1058–1065 (2020).
14. P. Song, R. Wang, J. Zhu, T. Wang, Z. Bian, Z. Zhang, K. Hoshino, M. Murphy, S. Jiang, and C. Guo, "Super-resolved multispectral lensless microscopy via angle-tilted, wavelength-multiplexed ptychographic modulation," Opt. Lett. **45**(13), 3486–3489 (2020).
15. G. Zheng, R. Horstmeyer, and C. Yang, "Wide-field, high-resolution Fourier ptychographic microscopy," Nat. Photonics **7**(9), 739–745 (2013).
16. S. Dong, R. Horstmeyer, R. Shiradkar, K. Guo, X. Ou, Z. Bian, H. Xin, and G. Zheng, "Aperture-scanning Fourier ptychography for 3D refocusing and super-resolution macroscopic imaging," Opt. Express **22**(11), 13586–13599 (2014).
17. C.-H. Lu, C. Barsi, M. O. Williams, J. N. Kutz, and J. W. Fleischer, "Phase retrieval using nonlinear diversity," Appl. Opt. **52**(1), D92–96 (2013).
18. C. Zuo, J. Li, J. Sun, Y. Fan, J. Zhang, L. Lu, R. Zhang, B. Wang, L. Huang, and Q. Chen, "Transport of intensity equation: a tutorial," Optics and Lasers in Engineering **135**, 106187 (2020).
19. A. M. Maiden and J. M. Rodenburg, "An improved ptychographical phase retrieval algorithm for diffractive imaging," Ultramicroscopy **109**(10), 1256–1262 (2009).
20. P. Thibault, M. Dierolf, O. Bunk, A. Menzel, and F. Pfeiffer, "Probe retrieval in ptychographic coherent diffractive imaging," Ultramicroscopy **109**(4), 338–343 (2009).
21. P. Song, S. Jiang, H. Zhang, Z. Bian, C. Guo, K. Hoshino, and G. Zheng, "Super-resolution microscopy via ptychographic structured modulation of a diffuser," Opt. Lett. **44**(15), 3645–3648 (2019).
22. X. Ou, G. Zheng, and C. Yang, "Embedded pupil function recovery for Fourier ptychographic microscopy," Opt. Express **22**(5), 4960–4972 (2014).
23. A. Pan, C. Zuo, and B. Yao, "High-resolution and large field-of-view Fourier ptychographic microscopy and its applications in biomedicine," Rep. Prog. Phys. **83**(9), 096101 (2020).
24. E. J. Candes, Y. C. Eldar, T. Strohmer, and V. Voroninski, "Phase retrieval via matrix completion," SIAM Rev. **57**(2), 225–251 (2015).
25. E. J. Candes, X. Li, and M. Soltanolkotabi, "Phase retrieval from coded diffraction patterns," Applied and Computational Harmonic Analysis **39**(2), 277–299 (2015).
26. D. R. Luke, "Phase retrieval, what's new," SIAG/OPT Views and News **25**, 1–5 (2017).

Biomedical Optics EXPRESS

27. V. Bianco, B. Mandracchia, J. Běhal, D. Barone, P. Memmolo, and P. Ferraro, "Miscalibration-tolerant Fourier Ptychography," IEEE J. Sel. Top. Quantum Electron. **27**(4), 1–17 (2021).
28. S. Montrésor, P. Memmolo, V. Bianco, P. Ferraro, and P. Picart, "Comparative study of multi-look processing for phase map de-noising in digital Fresnel holographic interferometry," J. Opt. Soc. Am. A **36**(2), A59–A66 (2019).
29. Y. Choi, C. Yoon, M. Kim, W. Choi, and W. Choi, "Optical imaging with the use of a scattering lens," IEEE J. Sel. Top. Quantum Electron. **20**(2), 61–73 (2014).
30. J. K. Adams, V. Boominathan, B. W. Avants, D. G. Vercosa, F. Ye, R. G. Baraniuk, J. T. Robinson, and A. Veeraraghavan, "Single-frame 3D fluorescence microscopy with ultraminiature lensless FlatScope," Sci. Adv. **3**(12), e1701548 (2017).
31. N. Antipa, G. Kuo, R. Heckel, B. Mildenhall, E. Bostan, R. Ng, and L. Waller, "DiffuserCam: lensless single-exposure 3D imaging," Optica **5**(1), 1–9 (2018).
32. D. Batey, T. Edo, C. Rau, U. Wagner, Z. Pešić, T. Waigh, and J. Rodenburg, "Reciprocal-space up-sampling from real-space oversampling in x-ray ptychography," Phys. Rev. A **89**(4), 043812 (2014).
33. A. Maiden, D. Johnson, and P. Li, "Further improvements to the ptychographical iterative engine," Optica **4**(7), 736–745 (2017).